Proceedings Paper:
Thomas, D.W.P., Denton, A., Benson, T.M. et al. (6 more authors) (2001) Electromagnetic coupling to an enclosure via a wire penetration. In: Electromagnetic Compatibility, 2001. EMC. 2001 IEEE International Symposium on. , pp. 189-188.

https://doi.org/10.1109/ISEMC.2001.950588

ELECTROMAGNETIC COUPLING TO AN ENCLOSURE VIA A WIRE PENETRATION

D W P Thomas, A Denton, T M Benson, C Christopoulos, J Paul
The University of Nottingham,
University Park,
Nottingham, UK.

T Konefal, J F Dawson, A C Marvin, S J Porter
The University of York,
York,UK

Abstract: This paper presents an efficient model, which can be computed in seconds, for the coupling of external electromagnetic fields to the contents of an enclosure via wire penetrations. The coupling path accounts for the coupling of an external electric field to a wire penetration that establishes an internal electric field via the connect and internal wire segment. The internal electric field then couples onto another victim wire segment, inside the box. The accuracy of the model is demonstrated by the good agreement obtained between predicted induced voltage on the victim wire segment, and experimental measurements.

Introduction

An important mechanism for the coupling of electromagnetic fields to the interior of an enclosure is through wire penetrations. This paper presents an efficient and accurate model for this type of coupling. An external electromagnetic field induces a current onto an external wire which penetrates an enclosure via a connector. The current on the internal segment of the wire penetration will then excite an internal electromagnetic field in the form of propagating and evanescent waveguide modes within the enclosure. The internal electromagnetic fields can also induce currents on other structures within the enclosure and in this work another wire segment, or monopole is considered.

In the model described, the wire penetrations are represented as monopoles. Equivalent circuits for these monopoles, external source and a transmission line representation of the enclosure waveguide modes are used to represent the complete coupling path. It is generally accepted [1,2] that the method of moments (MoM) [3] gives accurate results for the impedance of dipole or monopole antennas. We have, therefore, used an empirical approximation for the monopole equivalent circuit impedance and effective length (hence antenna factor). This approximation is derived from the analysis of a number of MoM simulations and is similar to that proposed in [4, 5]. This equivalent circuit for the monopole is then incorporated into an equivalent circuit model of the coupling of the electromagnetic fields to the wire penetrations and for the excitation of the enclosure internal electromagnetic fields [6].

Theory

The problem studied is as depicted in Fig. 1. In Fig. 1 an external field impinges on an external wire (monopole A) protruding from a cuboidal box. The wire passes through a BNC connector to a second shorter wire (monopole B) inside the box. The second wire excites electromagnetic fields within the box and these are sensed by a third wire (monopole C). The signal picked up by wire C is passed to a receiver (network analyser) via a 50Ω coaxial cable where the received power is measured. In the analysis of this experiment antenna models of the wires are produced and a model for the electromagnetic coupling of the wires within the box are developed.

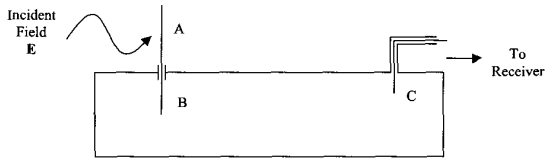

Figure 1 Experimental arrangement studied

Wire radiators

Wire radiators affect EMC by emitting and absorbing radiation in the same way as monopole/dipole antennas. Thus to describe a wire radiator in circuit solutions of EMC problems, the antenna-like properties of the wire are represented by an equivalent circuit in combination with an effective length function. To enable an efficient computational solution of the circuit model, the frequency-dependent impedance and effective length functions are approximated using simple expressions. As described in [4], the variation of a dipole's input impedance over a wide frequency range can be modelled as an equivalent circuit containing frequency dependent lumped elements. Further research along these lines by [5] identified the four element circuit model used in this paper. To the authors' knowledge, an approximation to the frequency-dependent effective length function has not previously appeared in the literature. Fig. 2 shows the model of a dipole (monopole) antenna: Using s to represent the complex frequency, $E^i(s)$ is the component of the incident electric field polarised in the direction of the antenna, $h_e(s)$ is the frequency-dependent effective length function, $Z_d(s)$ is the self impedance, $Z_L(s)$ is the load impedance and the voltage developed across the load is $V_L(s)$.

From Fig. 2, the antenna factor is

$$AF(s) = -\frac{E^i(s)}{V_L(s)} = \frac{Z_d(s) + Z_L(s)}{h_e(s) Z_L(s)} \quad (1)$$

Thus the calculation of the voltage $V_L(s)$ across a known load requires knowledge of both the self-impedance $Z_d(s)$ and the effective length function $h_e(s)$.

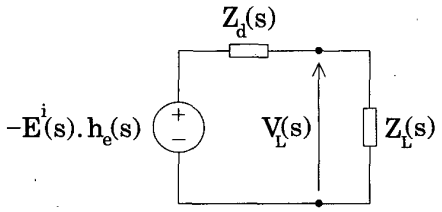

Figure 2 Dipole (monopole) antenna model

Fig. 3 shows the geometry and the four-element circuit model of the self impedance of a dipole developed by [5]: The tip-to-tip length is *2h* and the diameter is *2a*. The equivalent circuit consists of the electrostatic capacitance C_0 in series with a parallel combination of C_1, L_1 and R_1.

The circuit model of the dipole yields

$$Z_d = \frac{1}{sC_0} + \frac{s\frac{1}{C_1}}{s^2 + s\frac{1}{C_1R_1} + \frac{1}{L_1C_1}} \quad (\Omega) \quad \textbf{(2)}$$

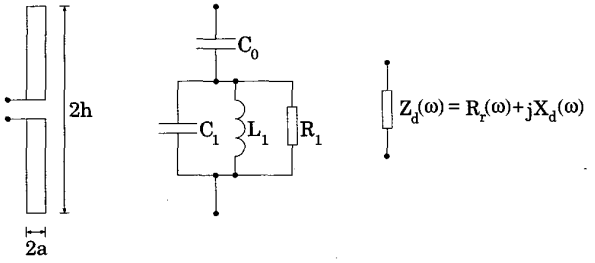

Figure 3 Geometry and self impedance model of a dipole antenna

As shown in Fig. 3, by putting $s=j\omega=j2\pi f$ (2) has the form $Z_d(f) = R_r(f) + jX_d(f)$ where $R_r(f)$ is the radiation resistance and $X_d(f)$ is the dipole reactance. This is then fitted to the self impedance obtained using MoM. The low frequency fitting point is chosen as the half-wave resonant frequency $f_0 \approx c/4h$, where $R_r(f_0) = R_0 \approx 72\Omega$ and $X_d(f_0) = 0$. The high frequency point is selected as the full-wave resonance frequency $f_1 \approx c/2h$, where $R_r(f_1) = R_1$ the first maximum value of the radiation resistance. The expressions we have derived differ from [5] because their goal was to approximate the low frequency impedance accurately, whereas we have constructed a model which approximates the self-impedance up to the full-wave resonant frequency. The empirical coefficients are then (with empirical values in the square brackets)

$$f_0 \approx \frac{[1.151]\ln(h/a) + [64.71]}{h} \quad (\text{MHz}) \quad \textbf{(3)}$$

$$f_1 \approx \frac{[8.401]\ln(h/a) + [87.67]}{h} \quad (\text{MHz}) \quad \textbf{(4)}$$

$$C_0 \approx \frac{[27.88]h}{\ln(h/a) - [1.452]} \quad (\text{pF}) \quad \textbf{(5)}$$

$$Z_{c0} \approx [70.88](\ln(h/a) - [0.7648]) \ (\Omega) \quad \textbf{(6)}$$

$$Z_{c1} \approx [125.2](\ln(h/a) - [1.768]) \ (\Omega) \quad \textbf{(7)}$$

$$R_0 \approx 72 \ (\Omega), \ R_1 \approx \frac{Z_{c0}^2}{R_0} \ (\Omega) \quad \textbf{(8)}$$

$$L_1 \approx \frac{Z_{c1}}{2\pi f_1} \ (\text{H}), \ C_1 \approx \frac{1}{2\pi f_1 Z_{c1}} \ (\text{F}) \quad \textbf{(9)}$$

Up to the full wave resonant frequency f_1 the effective length may be approximated using

$$h_e(s) = \frac{h\omega_h^2}{s^2 + s2\delta_h + \omega_h^2} \quad \textbf{(10)}$$

where it is found that the effective length resonant frequency $f_h = \omega_h/2\pi$ is

$$f_h \approx \frac{[7.609]\ln(h/a) + [92.57]}{h} \quad (\text{MHz}) \quad \textbf{(11)}$$

and the damping frequency is

$$\delta_h \approx \frac{h\omega_h}{2|h_e|_{\max}} \quad (\text{rads/s}) \quad \textbf{(12)}$$

where

$$|h_e|_{\max} \approx h\left([0.7063]\ln(h/a) + [0.1387]\right) \ (\text{m}) \quad \textbf{(13)}$$

Fig. 4 compares the self-impedance of a typical dipole obtained using MoM with the equivalent circuit model and Fig. 5 compares the effective length of a typical dipole obtained using MoM with the values given by (3).

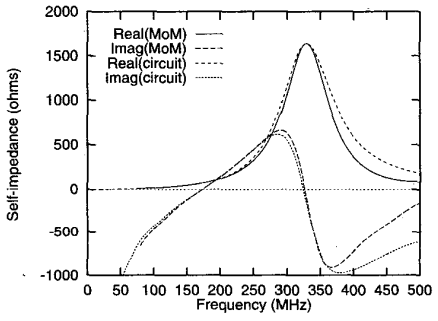

Figure 4 Self-impedance of a dipole antenna (*2h*=0.8189m, *2a*=3.0mm).

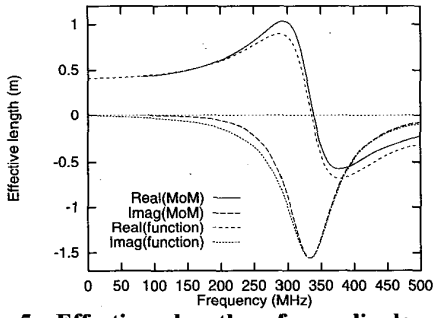

Figure 5 Effective length of a dipole antenna (*2h*=0.8189m, *2a*=3.0mm).

For a monopole above ground the self-impedance and effective length is exactly half of that given by (2) and (10) where h is the monopole length.

Electric dipole coupling to waveguide

Inside a metallic enclosure a wire penetration will excite electromagnetic fields as waveguide modes. Consider a short current carrying wire element AB (electric dipole) which is placed inside the waveguide in the near constant plane $z=z_c$, of any orientation, and let the waveguide be short circuited at $z=0$ and $z=-d$. Using the transmission line analogy, the schematic equivalent circuit for a particular mode n is as in Fig. 6. A voltage on the transmission line will induce a current on the dipole. Likewise, a voltage on the dipole will induce a current in the transmission line. The principle of reciprocity dictates that the magnitude of these effects are the same, so that we can model the interaction by a mutual capacitance C where

$$I_{dip} = j\omega C V_{WG} \qquad (14)$$

$$I_{WG} = j\omega C V_{dip} \qquad (15)$$

In (14) and (15) the currents, voltages and capacitance are all considered to act in the plane $z=z_c$, the location of the dipole or wire element. This is a reasonable assumption if the dipole is short or if it is oriented in the x-y plane. Considering the electric fields of a mode n (TE or TM) produced by the forward voltage $V_f^{0(n)}$ and reverse voltage $V_r^{0(n)}$ on the transmission line,

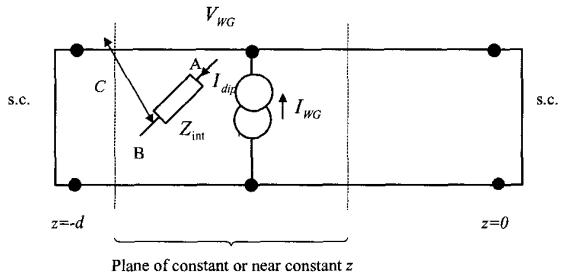

Figure 6. Schematic equivalent circuit for electric coupling of current element to waveguide, indicating the role of the mutual capacitance *C*.

we can write the induced current on the dipole as

$$I_{dip}^{(n)} = j\omega C^{(n)}\left(V_f^{0(n)}e^{-\gamma z} + V_r^{0(n)}e^{+\gamma z}\right) = \frac{V_A - V_B}{Z_{\text{int}}}$$

$$= \frac{1}{Z_{\text{int}}}\int_A^B \mathbf{E}^{(n)}.\mathbf{dl} \qquad (16)$$

where $\mathbf{E}^{(n)}$ is the combined electric field produced by both forward and reverse voltages of mode n. The voltage reflection coefficient $V_r^{0(n)} / V_f^{0(n)}$ is equal to -1 for a short circuit at $z=0$. Since the forward and reverse components of $\mathbf{E}^{(n)}$ depend linearly on $V_f^{0(n)}$ and $V_r^{0(n)}$ respectively, both of these terms can be eliminated from (16), enabling the mutual capacitance $C^{(n)}$ to be calculated. Details of this calculation are shown in [9]. Z_{int} is the self-impedance of the wire element given by (2).

Wire to waveguide mode coupling

Consider the first N lowest order modes, each with its own mutual capacitance $C^{(n)}$ to the electric dipole, located in the plane $z=z_c$ ($n=1....N$). For a transmission line voltage in mode n of $V_{WG}^{(n)}(z)$, the induced current in the dipole is

$$I_{dip}^{(n)} = j\omega C^{(n)} V_{WG}^{(n)}(z_c) \qquad (17)$$

Assuming that in the absence of a cavity the wire element or dipole carries a current I_{source}, the dipole currents from each mode combine with I_{source} to produce a total current on the dipole of

$$I_{Tot} = I_{source} + \sum_{n=1}^{N} I_{dip}^{(n)} \qquad (18)$$

The back current source in transmission line k (see Fig. 5) is then given by

$$I_{WG}^{(k)} = j\omega C^{(k)} Z_{\text{int}} I_{Tot} \qquad (19)$$

In this way, a single voltage on one transmission line will induce a voltage in every other transmission line, and the modes are properly coupled. The electric dipole itself is characterised by I_{source}, and Z_{int}.

The arrangement for the receiving wire penetration has an equivalent circuit comprising of two monopoles, one external (monopole A) with self-impedance Z_A and one internal (monopole B) with self impedance Z_B , as shown in Fig 7. The capacitance for the BNC connector can be found from standard equations [7] and was calculated to be 1.39 pF. This is used to derive the source current as from rearranging (1) we have

$$I_{source} = \frac{Eh(j\omega)}{Z_A + Z_B(1 + j\omega C_{BNC} Z_B)} \qquad (20)$$

The complete input circuit for the internal section of wire penetration is then as given in Fig. 8. The voltage source in Fig. 7 is replaced by the current source I_{source} (20) in series with the self-impedance Z_B. This then is coupled to a current source I_{dip} representing the coupling of the internal fields to the wire (monopole B).

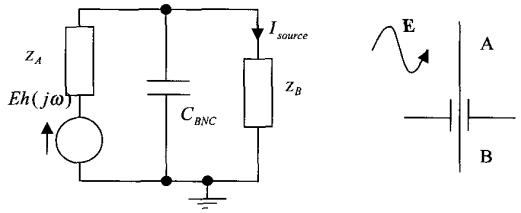

Figure 7. Equivalent circuit for wire penetration as two monopoles joined through a metal plat via a BNC socket

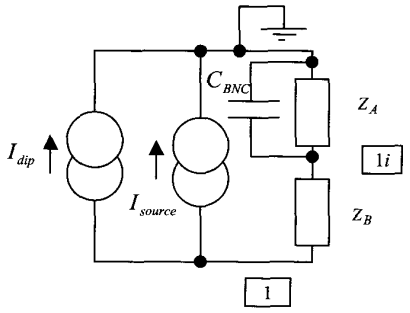

Figure 8. Equivalent input circuit for wire penetration in an enclosure.

Multimode wire to wire coupling

The equivalent circuit of Fig. 8 may be extended to include two wires, and to take into account several modes of propagation. Figure 9 illustrates the resulting equivalent circuit, where for simplicity only two modes are shown, the TE_{10} and TE_{20} modes. There are eight nodes in Fig. 9, labelled 1, 1*i*, 2, 2*i*, A1, A2, B1 and B2. The pair of dependent current sources labelled I_{wgB1} and I_{dipB1} effect the mutual coupling of the source wire (monopole B) to the waveguide via the TE_{10} mode (14) and (15). Similarly, coupling of the victim wire (monopole C) to the waveguide via the TE_{10} mode is achieved by I_{wgC1} and I_{dipC1}. The source wire (monopole B) couples to the TE_{20} mode by means of current sources I_{wgB2} and I_{dipB2}, whilst I_{wgC2} and I_{dipC2} provide the required TE_{20} coupling for the victim wire (monopole C). Note the mechanism by which mode coupling takes place between the TE_{10} and TE_{20} modes. Currents such as I_{dipB1} and I_{dipB2} flow through a common impedance of Z_B in series with the parallel combination Z_A and the connector capacitance C_{BNC}, inducing a voltage $Z_B I_{Tot}$ across the wire monopole impedance Z_B. This voltage then induces currents on both the TE_{10} and TE_{20} analogous transmission lines, via the current sources I_{wgB1} and I_{wgB2}. The latter two current sources are the circuit implementations of (19) with k referring to the TE_{10} and TE_{20} modes respectively.

The circuit may easily be extended to include higher order modes. For each additional mode n, an extra analogous transmission line is added to the circuit (with its associated current sources and impedances), similar to the two transmission lines illustrated in Fig. 9. Two extra current sources, one across I_{dipB} and the other across I_{dipC}, are also added to the circuit for every additional mode considered. These extra current sources provide the coupling of the voltage on the analogous transmission line for mode n to the source and victim wires illustrated in Fig. 9, as prescribed by (17). They are linearly dependent on the mutual capacitances $C_B^{(n)}$ and $C_C^{(n)}$ between the analogous transmission line and the source and victim wires respectively. The process of current combination described by (18) takes place on both the input and output circuits of Fig. 8, while completion of the mode coupling process described by (19) is effected by current sources such as I_{wgB1} and I_{wgC1} which are strapped across the analogous transmission lines. Once again, I_{wgB1} and I_{wgC1} are linearly dependent on $C_S^{(n)}$ and $C_V^{(n)}$ respectively.

The mutual capacitance for waveguide mode mn for the source wire (monopole B) can be derived from (16) and can be reduced to

$$C_{Bmn} = \frac{\mu_0 sa(-0.05)}{Z_{mn}\pi(Z_B + \frac{Z_A}{1+j\omega C Z_A})} \qquad (21)$$

The victim wire is loaded by the 50Ω cable impedance. The mutual capacitance of the victim wire (monopole C) for waveguide mode mn, found from (16), and can be reduced to

$$C_{Cmn} = \frac{\mu_0 sa(-0.05)}{Z_{mn}\pi(Z_C + 50)} \qquad (22)$$

where the waveguide width is a and terms s and transverse wave impedance Z_{mn} are defined in the appendix.

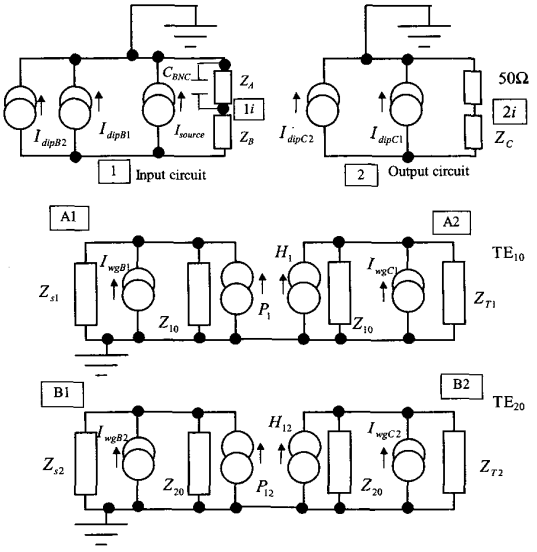

Figure 8. Equivalent circuit for wire to wire coupling inside an enclosure

For each transmission line, current sources P, H and impedances Z_{mn} represent the Norton equivalent circuit of the section of transmission line between the two wire monopoles. For example, for the TE_{10} analogous transmission line of Fig. 8, we have $P_1 = T_2 V_{A1} + T_1 V_{A2}$ and $H_1 = T_1 V_{A1} + T_2 V_{A2}$ where $T_1 = \frac{1}{Z_{10}\sinh(\gamma_{10}h)}$ and $T_2 = \frac{1}{Z_{10}}(1-\coth(\gamma_{10}h))$. Here h is the distance along the waveguide propagation axis between the two monopoles. This form of dependency for P and H is particularly useful for nodal analysis of the circuit. Z_{sn} and Z_{Tn} represent the impedances of the short circuited sections of transmission line between the wires and the two ends of the box. For example, $Z_{s2} = Z_{20}\tanh(\gamma_{20} l)$ where l is the distance of the source wire from the plane z=-d. Z_{mn} is taken as the transverse wave impedance of the mode [8].

The isolated wire results embodied in (17)-(19) must be modified slightly for the victim wire. Firstly, it should be recognised that the wire impedance Z_{int} of Fig. 8 is effectively connected to the lid of the box by the 50Ω resistance of the cable/network analyser combination used to extract energy from the box. Accordingly, when evaluating the coupling capacitance from (16), 50Ω is added in series with Z_{int}. Secondly, we note that the voltage across the 50Ω resistance of the output circuit of Fig. 8 does not actually appear inside the waveguide. Equations 14 and 15 must be modified slightly to reflect this. For example, in the case of coupling between the victim monopole and the TE_{10} transmission line, we write

$$I_{dipC} = j\omega C_{TE10}(V_{A2} + V_{2i}) \qquad (23)$$

$$I_{wgC} = j\omega C_{TE10}(V_{2i} - V_2) \qquad (24)$$

Equation 22 reflects directly the fact that the voltage across the 50Ω cable impedance is hidden from view as far as the waveguide is concerned. In (21), when the voltage V_{A2} is positive, the voltage V_{2i} is negative. Hence the additive sign in this equation to eliminate the effect of the 'hidden' voltage across the 50Ω resistance in the output circuit of Fig. 8. The remaining coupling capacitances and current sources are treated in a similar fashion for all the other modes considered. This complication arises in the theory simply because the wires cannot be totally isolated from the waveguide walls.

EXPERIMENTAL MEASUREMENTS

The full experimental arrangement inside the screened room and inside the anechoic chamber is as shown if Fig. 9. In the screened room a Log-periodic antenna was used and in the anechoic chamber a Bilog antenna was used. The external wire was 8cm long and the internal wires B and C were 5cm and 2.1 cm respectively. All wires are 0.8mm diameter and located along the centre line of the box ($x=a/2$). The initial box was of dimensions 29.2cm ×29.2cm×11.5cm. Below 700 MHz all the waveguide modes are evanescent. Between 700 MHz and 1GHz only the TE_{10} mode propagates. Also, since the source and victim wires are located along the box centre line, the TE_{10} is the dominant excited mode. The measurement results for the experiments performed in the screened room and anechoic chamber are shown in Fig. 10 and 11 compared with the theoretical results considering only the TE_{10} mode. The results show good agreement above 500 MHz. Below 500 MHz the results are masked by the noise level of the amplifier. The differences between Figs. 10 and 11 are due to the different antennas used and the different output powers of the amplifiers.

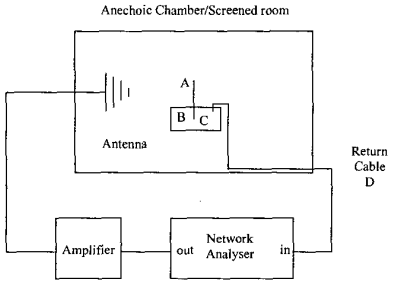

Figure 9. Experimental arrangement in the screened room and anechoic chamber

Only the TE_{10} mode was considered in the theoretical results of Fig. 10 and 11. The experiments of Fig. 10 and 11 were repeated using a larger box of dimensions 60cm×50cm×3cm. This larger box supported several propagating mode below 1GHz. The source and victim wires were also located off centre so that several modes were excited other than the TE_{10} mode. In this case wire A wise identical to the earlier experiments while wires B and C consisted of wire sections of length 5cm and diameter 1mm. In this case the TE and TM modes up to and including $m=4$ and $n=4$, is compared with the experimental results. The results are shown in fig. 12 and it again gives very good agreement between theory and experiment. Below 300 MHz the results are masked by the noise level of the amplifier.

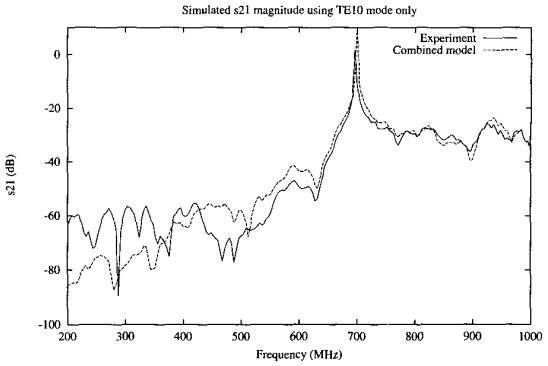

Figure 10. Experimental results from the screened room compared with the theoretical results.

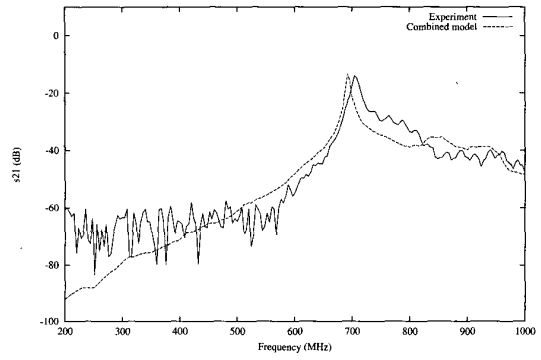

Figure 11. Experimental results from the anechoic chamber compared with the theoretical results.

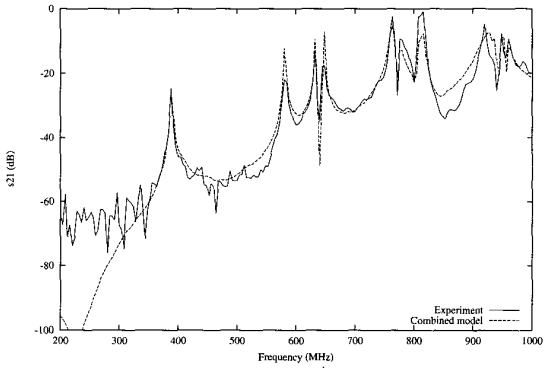

Figure 12 Experimental and theoretical results for the lager box in the anechoic chamber

CONCLUSIONS

A simple and efficient model has been developed for predicting the coupling of external fields to the enclosure contents via a wire penetration. Simple equivalent circuits have been derived for the

wire impedances and the coupling path. The results show excellent agreement with the experimental results carried out in two separate environments and two different box sizes.

REFERENCES

[1] M J Salter and M J Alexander. EMC antenna calibration and the design of an open field site. Measurement Science and Technology, 2:510-519, 1991.

[2] S F Kawalko and M Kanda. Effective length and input impedance of NIST standard dipoles. IEEE Transactions on Electromagnetic Compatibility, 39(4):404-408, November 1997.

[3] R F Harrington. Field computation by moment methods. Macmillan, NY, 1962.

[4] G W Streable and L W Pearson. A numerical study on realizable broad-band and equivalent admittances for dipole and loop antennas. IEEE Transactions on anteenas and propagation, 29(5):707-717, September 1981.

[5] T G Tang, Q M Tieng and M W Gunn. Equivalent circuit of a dipole antenna using frequency-independent lumped elements. IEEE Transactions on Antennas and Propagation, 41(1):100-103, January 1993.

[6] T Konefal, J F Dawson, A Denton, S J Porter, A C Marvin, T M Benson, C Christopoulos and D W P Thomas, Electromagnetic field predictions inside screened enclosures containing radiators EMC York 1999, IEE Pub. 464, July 1999, pp 95-100.

[7] Sander, K.F. and Reed, G.A.L., Transmission and propagation of electromagnetic waves, 2nd edition, Cambridge University Press, 1986.

[8] Collin, R.E., 'Field theory of guided waves,' 2nd edition, IEEE Press, New York, 1991.

Acknowledgements

The authors wish to thank EPSRC (Research grants GR/L-89723 and GR/L-89716), BAe BASE, Matra BAe Dynamics, ALSTOM Research and Technology Centre and Zuken-Redac for their support during this project.

APPENDIX 1

TE modes

$$Z_{mn} = \frac{j\omega\mu_0}{\gamma} \qquad \text{(A1)}$$

$$s = \left(\frac{Z_{mn}}{2\alpha_{mn}}\right)^{\frac{1}{2}} \qquad \text{(A2)}$$

$$\alpha_{mn} = \frac{\omega\mu_0\beta\dfrac{ab}{8}\left[\left(\dfrac{m\pi}{a}\right)^2(1-\delta_{m0})(1+\delta_{n0})+\left(\dfrac{n\pi}{b}\right)^2(1+\delta_{m0})(1-\delta_{n0})\right]_z}{\left[\left(\dfrac{m\pi}{a}\right)^2+\left(\dfrac{n\pi}{b}\right)^2\right]^2} \qquad \text{(A3)}$$

$$\beta_z = -j\gamma \qquad (\beta_z \text{ real and positive when } \omega > \omega_c) \qquad \text{(A4)}$$

$$\gamma = +\sqrt{\mu_0\varepsilon_0(\omega_c^2 - \omega^2)} \qquad \text{(A5)}$$

$$\omega_c^2\mu_0\varepsilon_0 = \left(\frac{m\pi}{a}\right)^2 + \left(\frac{n\pi}{b}\right)^2 \qquad \text{(A6)}$$

$$\rho_T = -1 \qquad \text{(A7)}$$

δ_{kl} is the Kronecker-delta symbol, equal to unity for $k = l$ and zero for $k \neq l$.

TM modes

$$Z_{mn}' = \frac{\gamma}{j\omega\varepsilon_0} \qquad \text{(A8)}$$